Journal of Engineering Mathematics **47:** 45–60, 2003.

Generalization of an asymptotic model for constant-rate aerosol reactors

B.D. SHAW
Mechanical and Aeronautical Engineering Department, University of California, Davis, CA 95616, U.S.A.
(e-mail: bdshaw@ucdavis.edu)

Received 4 June 2002; accepted in revised form 24 February 2003

Abstract. An asymptotic model was previously developed to predict behaviors of constant-rate aerosol reactors operating with particles in the free-molecular or continuum limits. This model considered the limiting cases of having either condensation or nucleation dominate during a nucleation burst that occurs from steady addition of condensable monomer. In the present article, this model is generalized to allow condensation and nucleation to both be important during a nucleation burst. Criteria are derived to predict the relative magnitudes of nucleation and condensation, and scaling relations are presented for particle number densities, particle sizes, and onset times and durations of nucleation bursts. Comparison of the asymptotic results with numerical integration of the governing equations is favorable both qualitatively and quantitatively.

Key words: aerosol, asymptotic, burst, condensation, nucleation.

1. Introduction

Nucleation and growth of particles from a vapor are important in many practical systems, for example, with formation of particulates in the atmosphere or production of powders for industrial use. Some systems generate condensable material over a short time period (*e.g.*, shock tubes). Others continuously transfer to or generate condensable material within a zone where appreciable nucleation occurs. These types of systems may be termed continuously reinforced reactors, the simplest of which is the constant-rate aerosol reactor, as described by Friedlander [1]. With the constant-rate aerosol reactor, condensable material is generated at a constant rate within the reactor. This reactor is assumed to be spatially uniform in composition, and to have temporally invariant temperatures and pressures (though the composition may change with time); smog chambers can sometimes approach conditions that are representative of constant-rate aerosol reactors [1].

In a previous paper, Shaw and Lawman [2] analyzed the constant-rate aerosol reactor using asymptotic methods. These analyses assumed that particles were either in the free-molecular or continuum regimes and that the aerosol was monodisperse. A variable present in nucleation-rate expressions was treated as a large parameter, and asymptotic analyses were developed in terms of this parameter. Scaling relations were presented for average particle sizes, particle number densities, and onset times and durations of nucleation bursts. The theory considered the limiting cases of having either condensation or nucleation dominate during a nucleation burst. The generalization of this theory, which is presented in this article, allows for nucleation and condensation to both be important during a nucleation burst.

Constant-rate aerosol reactors have been the subject of a number of other theoretical and computational studies. For example, Friedlander [1] has presented basic theory related to

these reactors. Friedlander [3] has also developed a set of ordinary differential equations to model the temporal variations of the moments of the aerosol distribution as well as the supersaturation of the condensable monomer. This model neglects coagulation and the Kelvin effect (*i.e.*, effects of particle size on vapor pressure) on condensation onto particles already nucleated, but makes no assumptions about the aerosol size distribution. Pratsinis *et al.* [4] have used the model of Friedlander [3] for computational studies of the characteristics of constant-rate aerosol reactors. They performed an approximate analysis to estimate regions of parameter space where coagulation and the Kelvin effect are safely negligible. In addition, Pratsinis [5] has computationally studied constant-rate aerosol reactors assuming a lognormal size distribution; Pratsinis allowed for coagulation in this analysis but did not consider the Kelvin effect. Warren and Seinfeld [6, 7] have presented computational results assuming that the aerosol-size distribution can be considered as monodisperse. In Warren and Seinfeld [6], the Kelvin effect is neglected as is coagulation, while in another article [7] the Kelvin effect is accounted for in an approximate manner. It is also noted that Shaw [8] has developed asymptotic solutions to the model of Friedlander [3].

Rao and McMurry [9] have presented a more general computational model for constant-rate aerosol reactors that uses a discrete-sectional approach, includes particle coagulation and the Kelvin effect, and allows for the assumption of the applicability of classical nucleation theory to be relaxed. This is in contrast to the other articles referenced above, which assume the applicability of classical nucleation theory (or related equations). Rao and McMurry [9] compared results from their model with the models of Friedlander [3] and Warren and Seinfeld [6] and concluded that conditions can exist where all three models produce roughly the same quantitative results as well as good qualitative agreement. This conclusion is important for the present paper, because it lends support to the idea that particle coagulation and the Kelvin effect may be neglected under certain conditions. It is noted, however, that Rao and McMurry [10] have suggested that the Tolman correction to surface tension (*i.e.*, variations in surface tension with particle size) may decrease the validity of this conclusion, though they also state that more work is needed in the area of particle-size-dependent surface tension to more fully validate their predictions. In addition, as noted above, Pratsinis *et al.* [4] have performed approximate analyses to determine conditions where coagulation and the Kelvin effect may be neglected. In the present paper, particle coagulation and the Kelvin effect are not considered in the analyses, and reactor conditions are assumed to lie within regions of parameter space where the Kelvin effect and particle coagulation may safely be neglected. Justification for these assumptions is presented in the following sections.

2. The governing equations

We start by presenting the evolution equations in dimensional form. Let S be the supersaturation of condensable monomer (*i.e.*, S is the ratio of the partial pressure of the condensable monomer to its saturation pressure). Also let M represent the mass generation rate of condensable monomer per unit volume, R the volumetric mass rate of nucleation of critical size clusters and C the volumetric mass rate of condensation of condensable monomers onto clusters larger than or equal to the critical size. Utilization of the ideal gas law then yields as the conservation equation for the mass of monomer in the gas phase, namely

$$\frac{m_1 P}{k_b T}\frac{\mathrm{d}S}{\mathrm{d}t} = M - R - C. \tag{1}$$

Here, T is absolute temperature, P is the total system pressure, m_1 the mass of a monomer molecule, k_b Boltzmann's constant and t time. Nucleation is assumed to be described by the classical theory of nucleation as described by Springer [11] such that

$$R = \alpha^2 S^2 \mathrm{e}^{-E/\log^2 S}, \tag{2}$$

where $\alpha = [2\psi/(\pi m_1)]^{1/2}[P/(k_b T)]^2 v_1 \rho V$, $E = 16\pi\psi^3 v_1^2/(3k_b T^3)$ and log denotes the natural logarithm. Equation (2) is valid for S greater than or equal to unity. For $S < 1$, $R = 0$. In Equations (1) and (2), ψ is the bulk liquid surface tension, v_1 the volume of a monomer molecule in the liquid phase, ρ the density of the condensed phase and V the volume of fresh nuclei (assumed constant). If the pressure and temperature are constant, α and E are constant.

A simplification that is made in the development of the asymptotic theory is that the diameters of freshly nucleated particles are constant. In order to apply this theory to an actual calculation, we must select an initial diameter, or equivalently, we must select a critical cluster number that will correspond to the number of monomers in a critical nucleus. The variable $g^* = [4\pi/(3v_1)][2\psi v_1/(k_b\ T\ \log\ S)]^3$ gives the number of monomers in a critical-size nucleus. Examination of this expression suggests that g^* will not vary strongly with S once the supersaturation exceeds a value of about 3. In calculations using the asymptotic results, a constant critical cluster number of 150 was assumed, which corresponds to $S = 3{\cdot}0474$. It is noted that the numerical results obtained from the asymptotic model will depend on the value selected for the critical cluster number. They do not vary strongly, however, and qualitative trends are essentially unaffected. As will be seen later, this selection for the critical cluster number provides good agreement between the asymptotic results and the results obtained from numerical integration of the more accurate model of Friedlander [3], especially for prediction of trends.

Condensation will be modeled using

$$C = \beta(S-1)d^2 N f, \tag{3}$$

where $\beta = \pi[m_1 P/(k_b T)](c_1/4)$. Equation (3) represents the difference between the rate that condensable vapor is absorbed by a particle and the rate that condensable vapor is evaporated from a particle. Here, c_1 is the average molecular speed of monomer molecules in the gas phase, N the number density of condensed particles and d the average diameter of condensed particles. For constant temperature and pressure, β is constant. The Kelvin effect has been neglected in Equation (3). Also, the function f is given by the Fuchs-Sutugin interpolation formula [6], which accounts for Knudsen number (Kn) effects, namely

$$f = \frac{1{\cdot}333\mathrm{Kn} + 1{\cdot}333\mathrm{Kn}^2}{1 + 1{\cdot}71\mathrm{Kn} + 1{\cdot}333\mathrm{Kn}^2}. \tag{4}$$

Here, $\mathrm{Kn} = 2\lambda/d$ where λ is the mean free path for monomer molecules in the gas phase. For this analysis we will consider the free-molecular limit ($\mathrm{Kn} >> 1$) and the continuum limit ($\mathrm{Kn} << 1$).

In this analysis we are interested in the early stages where particle formation is important, and we assume that appreciable particle coagulation occurs over long time scales and can be neglected over short time scales associated with monomer buildup and nucleation bursts. If coagulation is neglected, the particle number density is described by

$$\frac{\mathrm{d}N}{\mathrm{d}t} = \frac{R}{\rho V}. \tag{5}$$

To complete the formulation of the equations we need to develop an expression for the average particle diameter d. We will define the variable $G = \pi\rho N d^3/6$, which represents the total aerosol mass per unit volume and which also defines d. Based on conservation of mass, the following differential equation applies,

$$\frac{\mathrm{d}G}{\mathrm{d}t} = R + C. \tag{6}$$

If the dimensionless time $\tau = tk_bTM/(m_1P)$, dimensionless number density $n = Nk_bT\rho V/(m_1P)$ and dimensionless aerosol mass density $g = Gk_bT/(m_1P)$ are defined, Equation (1) can be expressed for the continuum and free-molecular limits as

$$\frac{\mathrm{d}S}{\mathrm{d}\tau} = 1 - AS^2\mathrm{e}^{-E/\log^2 S} - B(S-1)g^a n^b. \tag{7}$$

For Kn $>>$ 1 it is found that $B = (\beta/M)[6/(\rho\pi)]^{2/3}[m_1P/(k_bT)](\rho V)^{-1/3}$, $a = 2/3$ and $b = 1/3$ while for Kn $<<$ 1 the relations $B = 2{\cdot}67\lambda(\beta/M)(6/\pi)^{1/3}[m_1P/(k_bT)]\rho^{-1}V^{-2/3}$, $a = 1/3$ and $b = 2/3$ are found to apply. It is also noted that $A = \alpha/M$ is a constant. The first term on the right-hand side of Equation (7) (*i.e.*, unity) is the normalized and steady volumetric mass rate of addition of monomer. The second and third groups of terms in this equation represent dimensionless mass rates of nucleation ($AS^2\mathrm{e}^{-E/\log^2 S}$) and condensation ($B(S-1)g^a n^b$).

Using the previously defined variables allows Equations (5) and (6) to be transformed to the forms

$$\frac{\mathrm{d}g}{\mathrm{d}\tau} = AS^2\mathrm{e}^{-E/\log^2 S} + B(S-1)g^a n^b, \tag{8}$$

$$\frac{\mathrm{d}n}{\mathrm{d}\tau} = AS^2\mathrm{e}^{-E/\log^2 S}. \tag{9}$$

It is noted that the aerosol is assumed to be monodisperse but with sizes that vary with time. Coagulation is assumed to be negligible prior to and during a nucleation burst, *i.e.*, timescales for coagulation are assumed to be large relative to timescales for the approach to the nucleation burst as well as timescales associated with the duration of the nucleation burst itself. In addition, the Kelvin effect is neglected. Warren and Seinfeld [6] suggest that these assumptions (monodisperse aerosol, negligible coagulation, negligible Kelvin effect) provide appreciable simplifications and should not lead to large errors for predictions of behaviors prior to and during nucleation bursts. They should be verified, however, for the particular aerosol reactor that is to be modeled. The assumption of a monodisperse aerosol can be evaluated by comparison with numerical models that allow for polydisperse aerosols. Such comparisons have been provided by other researchers (*e.g.*, [5, 6, 9]), where it is shown that the assumption of a monodisperse aerosol should not introduce substantial errors for prediction of characteristics of aerosol reactors such as average particle sizes and number densities. In this paper, analytical results assuming a monodisperse aerosol are compared with numerical integrations of the more general model of Friedlander [3] that does not assume a monodisperse aerosol. As will be shown later, comparisons are favorable, both quantitatively and qualitatively.

Pratsinis *et al.* [4] have suggested that coagulation and the Kelvin effect can safely be ignored, provided that certain criteria are satisfied. For example, if coagulation is to be negligible over the time period Δt that corresponds to the time prior to and during a nucleation

Table 1. Model compound properties.

Property	Value	Units
T	298	K
W_1 (Mol. Wt.)	100	kg/kmole
ψ	0·025	N/m
n_s	$2{\cdot}43 \times 10^{14}$	m^{-3}
t_{coll}	45	s
ρ	1000	kg/m^3

burst, Δt must be small relative to the characteristic time $1/(N\zeta)$ for coagulation, where N is a characteristic aerosol number density and ζ is the collision frequency function. For the Kelvin effect to be negligible, Pratsinis *et al.* [4] also suggest that if the dimensionless surface tension group $\psi v_1^{2/3}/(k_b T)$ has values greater than 1·5, the Kelvin effect may be neglected without introducing appreciable errors. Relevant reactor/monomer conditions for the situations considered in the present paper are listed in Table 1, where we have listed conditions for a representative monomer compound investigated by Warren and Seinfeld [6] and Pratsinis [5]. The values in Table 1 yield the result that the dimensionless surface tension group $\psi v_1^{2/3}/(k_b T)$ has a value of 1·84 for the chosen conditions such that the Kelvin effect can be neglected. It is noted that in Table 1, t_{coll} represents a characteristic time between collisions of monomer molecules at the saturation number density n_s. This value for t_{coll} is calculated using the kinetic theory of gases.

Classical nucleation theory is expected to break down when the characteristic time n_s/Z for production of a monomer molecule is smaller than t_{coll}/S [6]. If we define the dimensionless monomer source rate $Z' = t_{\text{coll}} Z/n_s$, where Z is the volumetric generation rate of monomer molecules, we may roughly assume that classical nucleation theory begins to fail if Z' exceeds unity. In all of the calculations presented here, the variable Z' was never allowed to exceed unity. It is noted that by comparing their model with the simpler models of Friedlander [3] and Warren and Seinfeld [6], Rao and McMurry [9] suggest that if $2^{5/4}/(Z')^{1/2} >> 1$, the Kelvin effect should not be dominant, and that even when $2^{5/4}/(Z')^{1/2}$ is of order unity errors associated with neglecting the Kelvin effect should not be overriding. The range $2{\cdot}6 < 2^{5/4}/(Z')^{1/2} < 260$ applies for the specific conditions examined here. Using the above results as a guide, we only consider situations where coagulation and the Kelvin effect are both expected to be negligible.

For many situations of interest, it is not unusual for E to have values of 10^2 or larger. For example, the value $E = 103{\cdot}7$ applies to the model compound considered here (this value of E is used to generate all of the numerical results presented in this paper). Large values of E cause nucleation rates to be extremely sensitive to supersaturation values, and this sensitivity is exploited to provide the asymptotic analyses presented here.

Values for A and B are determined using the properties of the model compound listed in Table 1 as well as consideration of relevant values for monomer generation rates. The ratios $A/B = 448{\cdot}73$ and $A/B = 17900$ were employed for the free-molecular and continuum limits, respectively. The A and B values used to generate the numerical results in this article are the same as used in [2] (as is the value $E = 103{\cdot}7$). It is also noted that A is related to

Z' by the relation $A = [2\psi/(\pi m_1)]^{1/2} n_s T^2 v_1^2 \rho g^*/(m_1 Z')$. For the calculations presented in this paper, the variable A covers the range 10^2 to 10^6, which corresponds to a Z' range of $0{\cdot}84 \times 10^{-4}$ to $0{\cdot}84$ such that Z' never exceeded unity.

Equations (7)–(9) are to be solved with the initial conditions that there is no condensable vapor or any aerosol particles at time $\tau = 0$ such that $S(0) = g(0) = n(0) = 0$. It is also noted that Equations (7)–(9) are valid only for $S \geq 1$; for $S < 1$, $n = g = 0$. Thus, for $0 \leq \tau \leq 1$ it follows that $\mathrm{d}S/\mathrm{d}\tau = 1$, and hence $S = \tau$ for this early time period. For $\tau > 1$, nucleation and condensation rates are greater than zero (it is also noted that when solving the equations it is convenient to employ the initial conditions $S(1) = 1$ and $g(1) = n(1) = 0$, which follow from the early time behavior for $\tau \leq 1$). Inspection suggests, however, that the nucleation and condensation terms on the right-hand side of Equation (7) will be negligible relative to unity until S approaches a critical value that will be greater than unity. This critical value of S will be attained at a critical time τ_c, the value of which will be dependent upon the parameters A, B, E, a and b. Previous analysis [2] indicated that when $E >> 1$, the terms that describe nucleation and condensation in the sum $AS^2 \mathrm{e}^{-E/\log^2 S} + B(S-1)g^a n^b$ change very rapidly with time, and this sum approaches unity only when τ_c is approached very closely, at which time the approximation $S = \tau$ breaks down.

It is to be noted that when Equations (7)–(9) are numerically integrated, solutions for S display an initial period where S grows linearly with τ [2]. As a critical time is closely approached, however, and the nucleation burst begins, S values level off and begin to decrease. When S values drop slightly below the peak values attained, nucleation rates drop to negligible levels and the nucleation burst is concluded. The analyses presented here are concerned only with behaviors prior to and during a nucleation burst. For a description of behaviors after a nucleation burst, further analysis is necessary.

3. Asymptotic analysis

As noted previously, Equation (7) has the approximate solution $S = \tau$ until τ approaches τ_c closely. The approximation $S = \tau$ will be valid until the sum of the second and third terms in Equation (7) approaches unity. Because $E >> 1$, this will generally happen rather abruptly as a critical time τ_c is approached. Here, we define τ_c as occurring when

$$A\tau_c^2 \mathrm{e}^{-E/\log^2 \tau_c} + B(\tau_c - 1) g_c^a n_c^b = 1, \tag{10}$$

where g_c and n_c are the values of g and n at τ_c. We derive Equation (10) from Equation (7) by setting $\mathrm{d}S/\mathrm{d}\tau = 0$, providing a criterion for the time when the approximation $S = \tau$ becomes invalid. A nucleation burst occurs when τ approaches τ_c closely. Previously [2], one term or the other on the left-hand side of Equation (10) was assumed to be dominant. Here, we will allow for the possibility that each is of the same order. It is noted that if $A\tau_c^2 \mathrm{e}^{-E/\log^2 \tau_c} << 1$, condensation dominates during a nucleation burst, while if $(1 - A\tau_c^2 \mathrm{e}^{-E/\log^2 \tau_c}) << 1$, nucleation is most important during a nucleation burst.

To employ Equation (10) it is necessary to provide expressions for n and g as functions of τ (prior to the nucleation burst). As described elsewhere [2], this can be achieved by setting $S = \tau$ in Equations (8) and (9) and then solving the resulting equations asymptotically for $E >> 1$. For the variable n, the solution procedure involves solving the following differential equation:

$$\frac{\mathrm{d}n}{\mathrm{d}\tau} = A\tau^2 \mathrm{e}^{-E/\log^2\tau}. \tag{11}$$

A solution to Equation (11) can be developed by assuming a solution of the form $n = A\gamma \exp(-E/\log^2\tau)$, where γ is assumed to be a function of τ. Inserting this function into Equation (11) factors off the exponential term, yielding

$$\frac{\mathrm{d}\gamma}{\mathrm{d}\tau} + \frac{2E}{\tau\ \log^3\tau}\gamma = \tau^2. \tag{12}$$

We seek an asymptotic solution to Equation (12) for $E \to \infty$. For τ near unity, the right-hand-side of this equation will be of order unity. In developing the solution, we will assume that the term $2E\gamma/(\tau\ \log^3\tau)$ remains bounded as $\tau \to 1$. A way for this to happen is if $\gamma \approx \tau\ \log^3/(2E)$ for τ near unity. We may insert this expression into Equaiton (12) to find that $\mathrm{d}\gamma/\mathrm{d}\tau$ is of order $1/E$ relative to the other terms, which leads to the expansion $\gamma = \gamma_0/E + \gamma_1/E^2 + \cdots$. Inserting this expansion into Equation (12) and solving the resulting equations (which turn out to be algebraic equations and not differential equations), we have

$$\gamma = \frac{\tau^3\log^3\tau}{2E}\left[1 - \frac{3}{2E}(\log^2\tau + \log^3\tau) + \cdots\right]. \tag{13}$$

Use of the leading-order term in Equation (13) then yields the following asymptotic solution for n.

$$n \approx \frac{A}{2E}\tau^3(\log^3\tau)\mathrm{e}^{-E/\log^3\tau}. \tag{14}$$

An approximate solution for the variable g can be obtained by assuming $g = \phi n$ (where n is considered known) and $S = \tau$, yielding the following differential equation for ϕ when Equation (8) is considered, namely

$$\varepsilon\frac{\mathrm{d}\phi}{\mathrm{d}\tau} + \frac{1}{\tau\ \log^3\tau}(\phi - 1) = \Gamma(\tau - 1)\phi^a. \tag{15}$$

Here, $\varepsilon = 1/(2E)$ and $\Gamma = B/(2E)$. Equation (15) contains two parameters, ε and $\Gamma = \varepsilon B$. The parameter ε is small relative to unity and calculations indicate that Γ is of order unity or smaller, depending on the magnitude of B, which varies with the reactor conditions. If we treat ε as a small parameter and assume the expansion $\phi = \phi_0 + \varepsilon\phi_1 + \cdots$, the following expression is obtained for ϕ_0 when Γ is treated as order unity where it is assumed that $\phi \to 1$ as $\tau \to 1$. The assumption that $\phi \to 1$ as $\tau \to 1$ follows from Equations (8) and (9), which gives the result that $g \to 1$ as $S \to 1$ and

$$\phi_0 = 1 + \frac{B}{2E}\tau(\tau - 1)(\log\ \tau)^3\phi_0^a. \tag{16}$$

When Γ is assumed to be $\mathcal{O}(\varepsilon)$, the solution $\phi = 1 + [B/(2E)]\tau(\tau - 1)(\log\ \tau)^3 + \cdots$ is found via the expansion $\phi = \phi_0 + \varepsilon\phi_1 + \cdots$. However, since Equaiton (16) reduces to this solution for $\Gamma \to 0$, Equation (16) will be employed for the remainder of the analysis.

From Equation (16), we can find g using

$$g \approx n\phi_0, \tag{17}$$

where n is determined from Equation (14).

We now have the equations necessary to calculate τ_c. Consideration of Equations (10), (14), (16) and (17) produces the result that τ_c satisfies the following two equations:

$$A\tau_c^2 \mathrm{e}^{-E/\log^2 \tau_c}\phi_{0c} = 1, \tag{18}$$

$$\phi_{0c} = 1 + \frac{B}{2E}(\tau_c - 1)\tau_c(\log^3 \tau_c)\phi_{0c}^a. \tag{19}$$

Equation (18) shows that $\phi_{0c} = 1/(A\tau_c^2 \mathrm{e}^{-E/\log^2 \tau_c})$ so that if $\phi_{0c} >> 1$, nucleation rates are negligible relative to condensation rates in the vicinity of τ_c. Conversely, as $\phi_{0c} \to 1$, nucleation rates become increasingly important relative to condensation rates near τ_c. Equations (18) and (19) may be combined into the single relation

$$A\tau_c^2 \mathrm{e}^{-E/\log^2 \tau_c} + \frac{B}{2E}\tau_c(\tau_c - 1)(\log^3 \tau_c)(A\tau_c^2 \mathrm{e}^{-E/\log^2 \tau_c})^b = 1. \tag{20}$$

Given values for all other parameters, Equation (20) is to be solved by iteration for τ_c.

More accurate solutions of Equations (11) and (12) can be obtained by use of the method of strained coordinates [2]. This is worthwhile, since Equation (13) becomes less accurate for large values of τ (*i.e.*, Equation (13) is not uniformly valid), and using strained times increases the solution accuracy for large τ. To this end, we may define the strained times s and k [2] using

$$\tau = s + \frac{s}{2E}\log^3 s, \tag{21}$$

$$s = k + \frac{s_1}{2E}, \tag{22}$$

where

$$s_1 = \frac{\dfrac{\mathrm{d}\phi_0}{\mathrm{d}k} + \dfrac{\phi_0(k-2)+2}{k(k-1)}}{\dfrac{\phi_0 - 1}{k^2 \log^3 k}\left[1 + \dfrac{3}{\log k} + \dfrac{k}{k-1}\right]}, \tag{23}$$

$$\frac{\mathrm{d}\phi_0}{\mathrm{d}k} = \phi_0(\phi_0 - 1)\frac{\dfrac{1}{k} + \dfrac{1}{k-1} + \dfrac{3}{k \log k}}{\phi_0(1-a) + a}. \tag{24}$$

In terms of the strained times, Equations (14) and (16) are expressed as follows, where Equation (17) is unchanged,

$$n \approx \frac{A}{2E}s^3 \left(\log^3 s\right) \mathrm{e}^{-E/\log^2 \tau}, \tag{25}$$

$$\phi_0 = 1 + \frac{B}{2E}k(k-1)(\log k)^3 \phi_0^a. \tag{26}$$

If the s and k variables are used, calculation of g and n as a function of τ proceeds by first specifying a value of k. We then solve Equation (26) iteratively for ϕ_0, allowing s_1 to be calculated using Equations (23) and (24). The variables s and τ are then found by using Equations (21) and (22), which allows n and g to be calculated. To find n and g values at a specific time τ, k must be iterated. To evaluate Equation (10) when the s and k variables are employed, we first assume a value of k and then calculate the values of g, n and τ_c

that are associated with this k value. These values are substituted in the left-hand side of Equation (10). The assumed value of k would be iterated until the terms on the left-hand side of Equation (10) sum to unity. The strained times are employed to enable better estimates of τ_c to be made. The usefulness of the strained variable approach is considered later when we compare computational and asymptotic results.

For analysis of the solution behavior near τ_c, *i.e.*, when the approximation $S = \tau$ breaks down, we may rewrite Equations (7) and (9) in terms of appropriate stretched variables. Based on the prior analyses, we will use the information that solution behaviors prior to the nucleation burst are dominated by the exponential term $\mathrm{e}^{-E/\log^2 S}$, which can be expressed as $\mathrm{e}^{-E/\log^2 \tau_c}\ \mathrm{e}^{-E(1/\log^2 S - 1/\log^2 \tau_c)}$. If we consider only the term $\mathrm{e}^{-E(1/\log^2 S - 1/\log^2 \tau_c)}$, inspection shows that for $E >> 1$, this term is of order unity only if S approaches τ_c closely. The function $1/\log^2 S$ may be expanded in a Taylor series about $S = \tau_c$, yielding $1/\log^2 S = 1/\log^2 \tau_c - 2(S - \tau_c)/(\tau_c \log^3 \tau_c) + \cdots$. As a result, the function $\mathrm{e}^{-E/\log^2 S}$ can be expressed as shown below.

$$\mathrm{e}^{-E/\log^2 S} = \mathrm{e}^{-E/\log^2 \tau_c}\mathrm{e}^{-E(S-\tau_c)/(\tau_c\ \log^3 \tau_c)+\cdots}.$$

Based upon the above equation, we define the stretched variable $\sigma = 2E(S - \tau_c)/(\tau_c \log^3 \tau_c)$, which is a rescaled supersaturation that is of order unity when τ is near τ_c. By expressing S in terms of σ (*i.e.*, $S = \tau_c + (\tau_c\ \log^3 \tau_c)\sigma/(2E)$), and using this result in Equations (7) and (9), we find that a convenient rescaled time is given by $\eta = 2E(\tau/\tau_c - 1)/\log^3 \tau_c$, where η causes changes in σ to be of order unity over changes in η of order unity, *i.e.*, $\mathrm{d}\sigma/\mathrm{d}\eta \leq \mathcal{O}(1)$. We will also define $\omega = n/[A\tau_c^3 \log^3 \tau_c \mathrm{e}^{-E/\log^2 \tau_c}/(2E)]$, which is the aerosol number density rescaled to be of order unity for τ near τ_c, where it is to be noted that $n_c \approx A\tau_c^3 \log^3 \tau_c \mathrm{e}^{-E/\log^2 \tau_c}/(2E)$. If we note that $g = \tau - S$ and utilize the asymptotic expansions $\sigma = \sigma_0 + \sigma_1/E + \cdots$ and $\omega = \omega_0 + \omega_1/E + \cdots$, we can express the leading-order terms in the expansions of Equations (7) and (9) as

$$\frac{\mathrm{d}\sigma_0}{\mathrm{d}\eta} = 1 - r\mathrm{e}^{\sigma_0} - (1 - r)(\eta - \sigma_0)^a \omega_0^b, \tag{27}$$

$$\frac{\mathrm{d}\omega_0}{\mathrm{d}\eta} = \mathrm{e}^{\sigma_0}, \tag{28}$$

where $r = A\tau_c^2 \mathrm{e}^{-E/\log^2 \tau_c}$. The variable r represents the ratio of the rate that monomers are consumed by nucleation of fresh particles during a nucleation burst to the monomer generation rate. Examination of Equation (27) shows that for $r << 1$ condensation dominates during the nucleation burst, while for $(1 - r) << 1$ nucleation dominates during the nucleation burst. When $(1 - r)$ and r are both of order unity, condensation and nucleation rates are both important during the nucleation burst. Setting $r = 1$ or 0 in Equation (27) reproduces the equations solved by Shaw and Lawman [2] assuming that either nucleation or condensation dominates during the nucleation burst. By generalizing the analyses of Shaw and Lawman [2] we are now able to predict the relative magnitudes of nucleation and condensation during a nucleation burst, which was not possible using the original analysis. Figure 1 shows the behavior of r (obtained using Equation (20)) as a function of A for the free-molecular and continuum limits. As might be anticipated, r approaches unity when A becomes sufficiently small. As A grows, however, r rapidly becomes very small.

Equation (27) is to be solved subject to the matching condition $\lim_{\eta \to -\infty} \sigma_0 = \eta$ while Equation (28) must match Equation (25). A formal solution to Equation (28) may be written as

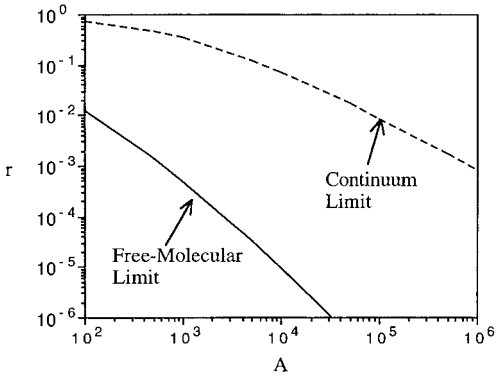

Figure 1. Plots of r as a function of A.

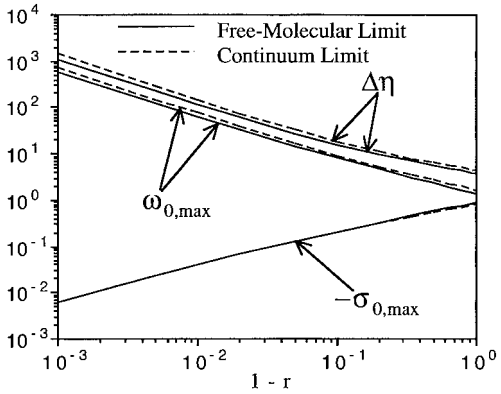

Figure 3. Plots of $\sigma_{0,\max}$, $\omega_{0,\max}$ and $\Delta\eta$ as a function of the quantity $1-r$ for the free-molecular and continuum limits.

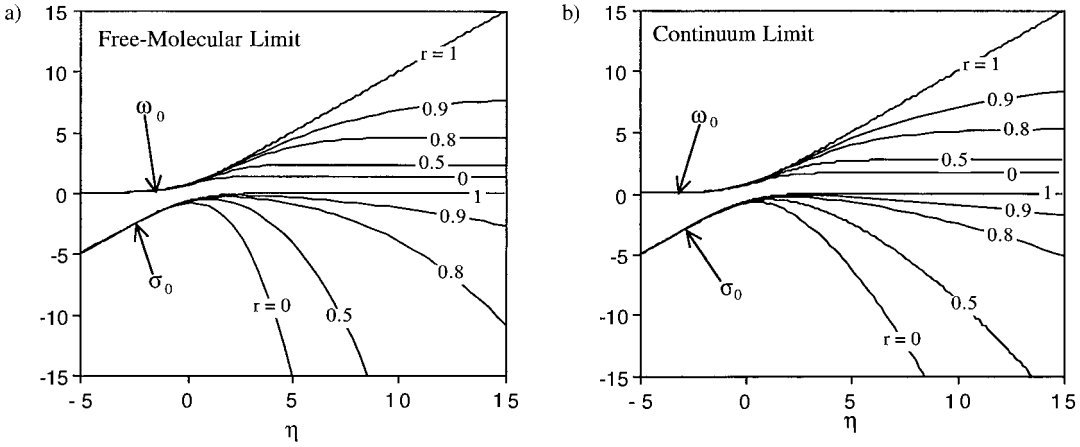

Figure 2 Solutions of Equations (27) and (28) for the (a) free-molecular and (b) continuum limits.

$\omega_0 = \int^{\eta} e^{\sigma_0} d\eta + C_1$ which reduces to $\omega_0 \approx e^{\eta} + C_1$ for $\eta \to -\infty$. Matching this relation to the leading-order expansion of Equation (25) gives $C_1 = 0$.

The nonlinear character of Equations (27) and (28) requires that solutions be found numerically, which necessitates defining appropriate initial (starting) conditions. To this end, we define $\theta = \eta - \sigma_0$. Inserting this relation into Equation (27) yields, for $\eta \to -\infty$

$$\frac{d\theta}{d\eta} = re^{\eta} + (1-r)\theta^a e^{\eta b}. \tag{29}$$

where $\omega_0 = e^{\eta}$ for $\eta \to -\infty$ has been used. Equation (29) has the solution $\theta = e^{\eta}$, where we have used the relation $a + b = 1$. We may then deduce that $\sigma_0 \approx \eta - e^{\eta}$ for $\eta \to -\infty$. Use of this asymptotic relation for σ_0 (as well as that provided above for ω_0) as a starting condition is necessary for developing accurate numerical solutions. When the numerical solutions were determined, the starting η value was varied until the results were independent of this value.

Figure 2 shows solutions of Equations (27) and (28) for the free molecular and continuum limits and for different values of r. These solutions, as well as all other numerical integrations

presented in this paper, were generated with a fourth-order Runge-Kutta scheme. In employing this scheme, we varied the time steps until time-step independent results were obtained. The Rung-Kutta scheme was implemented using double precision FORTRAN.

As might be anticipated, solutions for r near unity display an extended period of time for the nucleation burst, *i.e.*, $\mathrm{d}\omega_0/\mathrm{d}\eta$ is appreciable for long durations. For $r = 1$ we may obtain the exact solutions $\sigma_0 = -\log(1 + \mathrm{e}^{-\eta})$ and $\omega_0 = \log(1 + \mathrm{e}^{\eta})$, showing that for this case, ω_0 grows without bound as η increases. When $r < 1$, a limited period of time ($\Delta\eta$) is obtained where ω_0 grows rapidly; outside of $\Delta\eta$, changes in ω_0 are negligible. The period $\Delta\eta$ may be considered to be the duration of the nucleation burst. From Figure 2, it is evident that for the continuum and free-molecular limits, appreciable nucleation occurs roughly when $\sigma \geq -2$; when $\sigma_0 < -2$, changes in ω_0 are small. From the definition of the stretched time η, we may estimate the duration of the nucleation burst as

$$\Delta\tau \approx \frac{\tau_c \log^3 \tau_c}{2E} \Delta\eta, \tag{30}$$

where $\Delta\eta$ is defined to be the stretched time period where $\sigma_0 \geq -2$. Plots of $\Delta\eta$ as a function of $(1 - r)$ are shown in Figure 3.

Figure 3 also shows maximum values of ω_0 and σ_0 (*i.e.*, $\omega_{0,\max}$ and $\sigma_{0,\max}$) as a function of $(1 - r)$ that were calculated from numerical solutions of Equations (27) and (28) (note that the negative of $\sigma_{0,\max}$ is actually plotted). This figure is useful in that it allows estimates for the maximum supersaturation values ($S_{\max}$) and final particle number densities (n_{tot}) to be obtained from the asymptotic theory. From the definitions of the stretched variables σ and ω, we may derive the expressions,

$$S_{\max} \approx \tau_c \left(1 + \frac{\log^3 \tau_c}{2E} \sigma_{0,\max}\right), \tag{31}$$

$$n_{\mathrm{tot}} \approx \frac{\tau_c^3 \log^3 \tau_c}{2E} A \mathrm{e}^{-E/\log^2 \tau_c} \omega_{0,\max}, \tag{32}$$

which contain the variables $\sigma_{0,\max}$ and $\omega_{0,\max}$. Results using Equations (31) and (32) are shown in Figures 4 and 5, respectively. Also plotted are calculations of $S_{\max}$ and n_{tot} obtained from direct numerical integration of Equations (7)–(9). In these figures, the term 'leading-order theory' refers to the asymptotic theory where the approximation $\tau = s = k$ is used and Equation (20) is used to calculate τ_c, while the term 'higher-order theory' refers to calculating τ_c using the strained times s and k (with values different from τ) and employing the resulting value for r in Equations (27) and (28). The higher-order theory results for the most part fall closer to the numerical integration results than do the leading-order results. In general, the numerical and asymptotic solutions agree well over the range of A values considered, and in some cases it is difficult to distinguish between the numerical and asymptotic solutions. This is in contrast to the original research presented by Shaw and Lawman [2], where the continuum-limit solutions became invalid as A decreased in magnitude. This occurred because the original theory did not allow for the parameter r to have values between zero and unity.

Finally, as shown by Shaw and Lawman [2], the average particle diameter (d) may be expressed as

$$d = d_0 (g/n)^{1/3} \approx d_0 \phi_0^{1/3}, \tag{33}$$

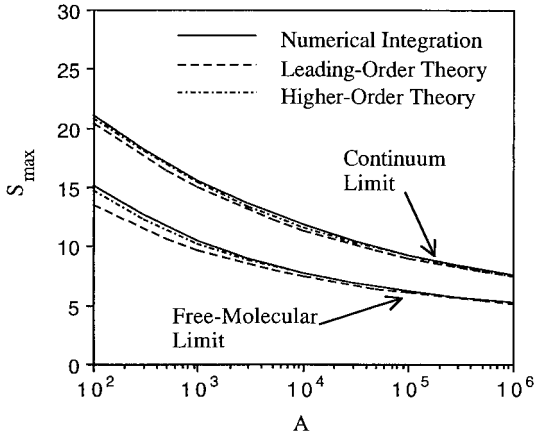

Figure 4. Plots of $S_{\max}$ as a function of A for the free-molecular and continuum limits.

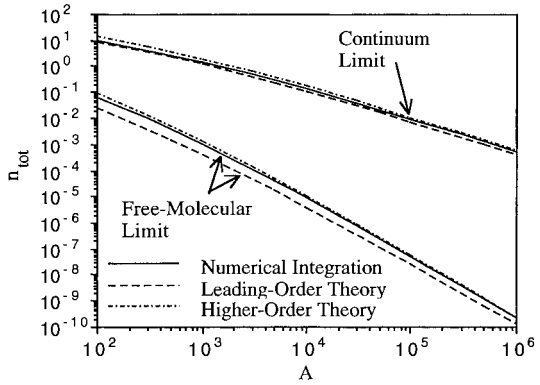

Figure 5. Plots of n_{tot} as a function of A for the free-molecular and continuum limits.

where d_0 is the diameter of freshly-nucleated particles (taken as constant). Equation (33) is valid prior to the nucleation burst (*i.e.*, for τ appreciably less than τ_c). If we express the ratio g/n in terms of η, σ, and ω and expand the result in powers of $1/E$, we obtain the following equation to describe particle size variations during a nucleation burst

$$\frac{d}{d_0} r^{1/3} \approx \left(\frac{\eta - \sigma_0}{\omega} \right)^{1/3} . \tag{34}$$

For $r = 1$, the exact solution presented earlier gives $[(\eta - \sigma_0)/\omega_0]^{1/3} = 1$. Numerical integrations show that over the duration of a nucleation burst (*i.e.*, when $\sigma_0 \geq -2$), $[(\eta - \sigma_0)/\omega_0]^{1/3}$ does not depend strongly on r, even as $r \to 0$. For example, when $r = 0$, $[(\eta - \sigma_0)/\omega_0]^{1/3}$ is calculated to have values of 1·45 and 1·43 for the free-molecular and continuum limits, respectively, when $\sigma_0 = -2$ at the end of the nucleation bursts (at the beginnings of the nucleation bursts, $[(\eta - \sigma_0)/\omega_0]^{1/3}$ is very close to unity for the free-molecular and continuum limits for all values of r). As r becomes larger, values of $[(\eta - \sigma_0)/\omega_0]^{1/3}$ become smaller and approach unity. Hence, the average particle size during a nucleation burst is approximately $d_0 r^{-1/3}$. From the definition of r, it can be seen that the functional form of this prediction for the average particle size during a nucleation burst is precisely the same as provided by Shaw and Lawman [2]. There is a significant difference between the two results, however, since the analysis presented in this paper allows for accurate prediction of r (and hence τ_c) when r is not small relative to unity. The previous theory was not valid as r approached a value of unity, while the theory presented here is valid for all values of r.

4. Comparison with a more accurate numerical model

In this section we compare the asymptotic results with a model advanced by Friedlander [3] for the dynamics of batch aerosol reactors operating in the free-molecular limit. This model provides evolution equations for the first three moments of the aerosol size distribution, and includes the effects of nucleation and condensation. In this model, the Kelvin effect is assumed to be negligible, as is coagulation of particles. However, no restrictions are placed upon the

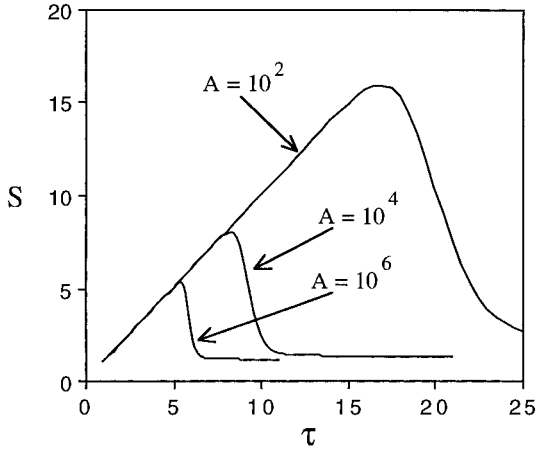

Figure 6. Plots of S as a function of τ obtained from integrating Equations (35)–(38).

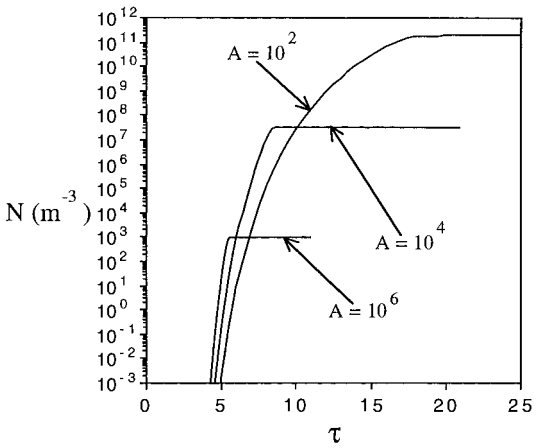

Figure 7. Plots of the number density N as a function of τ obtained from integrating Equations (35)–(38).

aerosol size distribution (it is allowed to evolve as determined by the conservation equations), and the critical nucleation diameter d_p^*, at which stable particles were nucleated, is allowed to vary according to the Kelvin relationship, namely, $d_p^* = 4\psi v_1/(k_b T \log S)$. The equations describing Friedlander's model are summarized below.

$$\frac{\mathrm{d}A_t}{\mathrm{d}t} = J(g^*)^{2/3}A_1 + 2\pi B_1(S-1)M_1, \tag{35}$$

$$\frac{\mathrm{d}M_1}{\mathrm{d}t} = Jd_p^* + B_1(S-1)N, \tag{36}$$

$$\frac{\mathrm{d}S}{\mathrm{d}t} = \frac{Z}{n_s} - \frac{Jg^*}{n_s} - (S-1)\frac{B_1A_t}{2v_1n_s}, \tag{37}$$

$$\frac{\mathrm{d}N}{\mathrm{d}t} = J. \tag{38}$$

Here, A_t is the total particle surface area per unit volume, M_1 is a moment of the aerosol size distribution, $B_1 = 2n_s v_1[k_bT/(2\pi m_1)]^{1/2}$, A_1 is the surface area attributed to a monomer molecule in the liquid phase, and J is the particle nucleation rate. In the calculations, the particle nucleation rate was assumed to be described by classical nucleation theory such that $J = \{[2\psi/\pi m_1]^{1/2}n_s^2 v_1\}S^2 \exp(-E/\log^2 S)$ where E is as previously defined in the asymptotic theory. Equations (35)–(38) were integrated numerically using a fourth-order Runge-Kutta scheme subject to the initial conditions $S(1) = 1$, $N(1) = 0$, $M_1(1) = 0$, and $A_t(1) = 0$. Results from these numerical integrations are compared below with the asymptotic models. It is noted that Equations (35)–(38) have not been rendered dimensionless.

The conditions under which Equations (35)–(38) were integrated correspond to the model compound considered by Warren and Seinfeld [6] and by Pratsinis [5] (Table 1). Shown in Figure 6 are values for the supersaturation S plotted as a function of the dimensionless time $\tau = tZ/n_s$; this definition of τ is identical to that employed earlier in this paper. These results were obtained by numerically integrating Equations (35)–(38). The qualitative features are

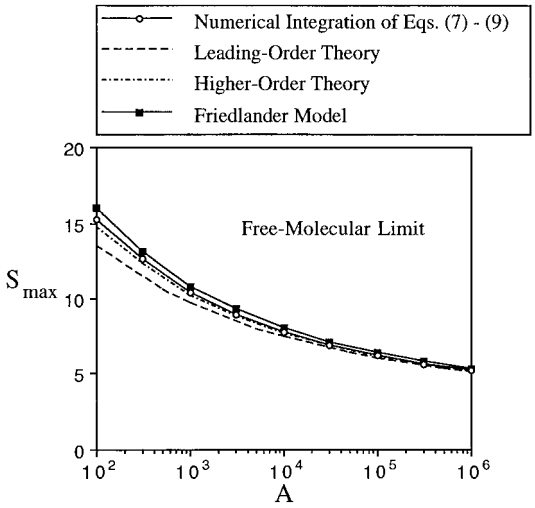

Figure 8. Comparison of predictions of the peak supersaturation S_{max} obtained from the asymptotic models as well as numerical integrations of the monodisperse aerosol model (Equations (7)–(9)) and numerical integrations of Equations (35)–(38).

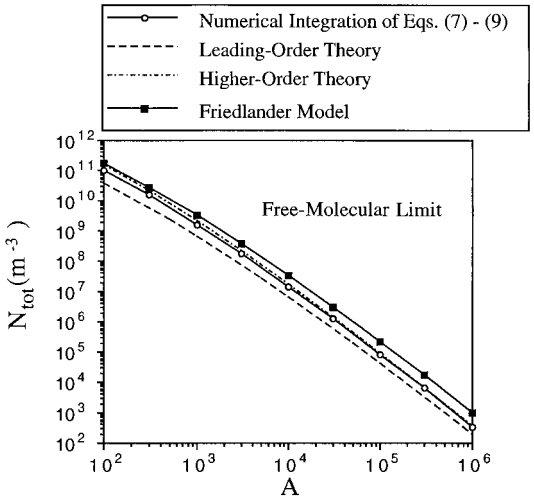

Figure 9. Comparison of predictions of the final number density N_{tot} obtained from the asymptotic models as well as numerical integrations of the monodisperse aerosol model (Equations (7)–(9)) and numerical integrations of Equations (35)–(38).

similar to what are found when the conservation equations describing monodisperse aerosols are numerically integrated [2]. For example, an initial period exists where S grows linearly with τ. This period is terminated rather abruptly when the supersaturation peaks sharply and then begins to decrease. Figure 7 shows calculated histories for particle number densities obtained by numerically integrating Equations (35)–(38). As would be anticipated, the number densities grow very rapidly until S peaks. After the supersaturation peaks, number densities then remain essentially constant because nucleation rates decrease in magnitude extremely rapidly as S values drop even slightly.

Figure 8 shows predictions for the peak supersaturation S_{max} attained as a function of the parameter A. Plotted in Figure 8 are numerical integrations of the Friedlander model (Equations (35)–(38)) and the leading-order and higher-order asymptotic results, as well as numerical integrations of Equations (7)–(9). The various models agree well, especially as the parameter A increases in magnitude, which corresponds to decreasing magnitudes of Z'.

Figure 9 shows plots of the final number density attained (N_{tot}) as a function of A, where N_{tot} has units of particles per cubic meter. Plotted are results obtained from numerical integrations of the Friedlander model (Equations (35)–(38)) and the leading-order and higher-order asymptotic results, as well as numerical integrations of Equations (7)–(9). In general, agreement between the various models is good, especially regarding qualitative trends over about eight orders of magnitude in predictions for number densities. Also, the quantitative results compare well with the lowest-order theory predicting final number densities that are typically within a factor of five of the results obtained from the Friedlander model; the higher-order theory as well as numerical integrations of Equations (7)–(9) are even closer.

Table 2 provides results for predictions of average particle diameters obtained from the leading-order and higher-order asymptotic theories and also from the Friedlander model.

Table 2. Comparison of average particle diameters from the asymptotic theories using the relation $d_0 r^{-1/3}$ and Equations (35)–(38). Listed are values of the parameter r and average diameters (d). The subscripts TH1, TH2 and F refer to results obtained from the leading-order theory, the higher-order theory, and Friedlander's model, respectively. The value $d_0 = 3{\cdot}62 \times 10^{-9}$ m was used in these calculations.

A	r_{TH1}	r_{TH2}	d_{TH1}(m)	d_{TH2}(m)	d_{F}(m)
10^2	$1{\cdot}22 \times 10^{-2}$	$4{\cdot}11 \times 10^{-2}$	$1{\cdot}57 \times 10^{-8}$	$1{\cdot}05 \times 10^{-8}$	$7{\cdot}75 \times 10^{-9}$
10^4	$9{\cdot}44 \times 10^{-6}$	$2{\cdot}27 \times 10^{-5}$	$1{\cdot}71 \times 10^{-7}$	$1{\cdot}28 \times 10^{-7}$	$8{\cdot}37 \times 10^{-8}$
10^6	$8{\cdot}32 \times 10^{-10}$	$1{\cdot}52 \times 10^{-9}$	$3{\cdot}85 \times 10^{-6}$	$3{\cdot}15 \times 10^{-6}$	$1{\cdot}98 \times 10^{-6}$

The average diameters listed for the Friedlander model correspond to average diameters that existed when the peak supersaturation $S_{\max}$ was achieved. The average diameters for the Friedlander model (d_F) were defined using the relation $d_F = [A_t/(\pi N)]^{1/2}$. The results listed in Table 2 indicate that the leading-order and higher-order asymptotic theories predict average particle diameters to within a factor of two for the particular problem considered. It is noted that the r values listed are all small relative to unity. These are the values that happened to occur for the particular conditions investigated. Other conditions may lead to r values that are of order unity.

The results listed in Table 2 were obtained assuming that particles were always within the free-molecular regime. For this to hold true, it is easily calculated that total aerosol reactor pressures must actually be quite low (a few Torr) for the largest particles considered; the smaller particles can withstand higher reactor pressures before the assumption of a free-molecular aerosol is violated.

For coagulation to be negligible, the timescale Δt for the onset and duration of the nucleation burst must be smaller than the characteristic time for coagulation $[1/(N\zeta)]$. Estimates suggest that $\Delta t << [1/(N\zeta)]$ for all of the calculations performed here. In making these estimates, ζ values for collision rates between hard spheres in the free-molecular limit [3] were used, where the spheres were assumed to have the diameters and number densities in Table 2 and Figure 9, respectively.

5. Conclusions

We have extended an asymptotic model that was developed to predict behaviors of constant-rate aerosol reactors operating with particles in the free molecular or continuum limits. This previous model was restricted to situations where either nucleation or condensation was dominant during a nucleation burst, but not both. This model has been generalized to cover the situation where both condensation and nucleation may be appreciable during a nucleation burst. The analysis identified the parameter r, which represents the ratio of the volumetric mass nucleation rate to the volumetric mass generation rate of monomers, as being important in determining behaviors during a nucleation burst. When r is small relative to unity, condensation dominates during a nucleation burst. Conversely, when r closely approaches unity nucleation is dominant during a nucleation burst. When r is between these limits, nucleation and condensation are both important during a nucleation burst.

The analyses have also provided improved scaling relations for particle number densities, average particle sizes, and onset times and durations of nucleation bursts. Results using these scaling relations showed that the parameter r plays an important role in determining factors such as nucleation burst durations.

In general, the asymptotic models compared favorably with direct numerical integrations of the governing equations for a monodisperse aerosol. Good agreement was also obtained when the asymptotic results were compared with numerical integrations of an aerosol model that allowed for polydisperse aerosols in the free-molecular regime. For example, good agreement was obtained regarding particle number densities, average particle sizes and maximum supersaturation values obtained during nucleation bursts.

It is to be recalled that the equations presented were derived assuming that particles are either in the free molecular or continuum regimes, that the Kelvin effect is negligible, and that coagulation is negligible over the timescales associated with the onset and duration of a nucleation burst. These assumptions should all be checked if the results presented here are applied to any particular situation.

This paper can be extended in several ways. For example, it would be worthwhile to extend the analyses to consider situations where the Kelvin and Tolman effects are significant. It would be interesting to consider variable monomer generation rates, which might occur when the chemical reactions that generate monomers vary with time. The analyses presented here have assumed that aerosol reactors are spatially uniform. It would be useful to consider situations where aerosol formation occurs in reactors that have spatial variations (both transient and steady state), such as in a laminar or turbulent jet. Finally, the model could be extended to include variable particle nucleation diameters. This would increase the accuracy of numerical results obtained using the asymptotic model.

References

1. S.K. Friedlander, The behavior of constant-rate aerosol reactors. *Aerosol Sci. Technol*. 1 (1982) 3–13.
2. B.D. Shaw and J. Lawman, Analysis of constant-rate aerosol reactors. *Aerosol Sci. Technol*. 20 (1994) 363–374.
3. S.K. Friedlander, Dynamics of aerosol formation by chemical reaction. *Ann. N.Y. Acad. Sci.* 404 (1983) 354–364.
4. S.E. Pratsinis, T.T. Kodas, M.P. Dudukovic and S.K. Friedlander, Aerosol reactor design: effect of reactor type and process parameters on product aerosol characteristics. *Ind. Eng. Chem. Process Des. Dev.* 25 (1986) 634–642.
5. S.E. Pratsinis, Simultaneous nucleation, condensation, and coagulation in aerosol reactors. *J. Colloid Interface Sci.* 124 (1988) 416–427.
6. D.R. Warren and J.H. Seinfeld, Nucleation and growth of aerosol from a continuously-reinforced vapor. *Aerosol Sci. Technol.* 3 (1984) 135–153.
7. D.R. Warren and J.H. Seinfeld, Prediction of aerosol characteristics resulting from a burst of Nucleation. *J. Colloid Interface Sci.* 105 (1985) 136–142.
8. B.D. Shaw, Asymptotic solution of nonlinear moment equations for constant-rate aerosol reactors. *Math. Prob. Eng.* 4 (1998) 233–246.
9. R.P. Rao and P.H. McMurry, Nucleation and growth of aerosol in chemically reacting systems: a study of the near-collision-controlled regime. *Aerosol Sci. Technol.* 11 (1989) 120–132.
10. R.P. Rao and P.H. McMurry, Effect of the Tolman surface tension correction on nucleation in chemically-reacting systems. *Aerosol Sci. Technol.* 13 (1990) 183–195.
11. G.S. Springer, Homogeneous nucleation. *Adv. Heat. Trans.* 14 (1978) 281–346.